A Systematic Design Methodology for Articulated Serpentine Robotic Tails to Assist Agile Robot Behaviors

Isaac Pressgrove

Thesis submitted to the faculty of the Virginia Polytechnic Institute and State University in partial fulfillment of the requirements for the degree of

Master of Science
In
Mechanical Engineering

Pinhas Ben-Tzvi, Chair
Corina Sandu
Steve Southward

May 11, 2022
Blacksburg, Virginia

Keywords: Robotic Systems, Design, Optimization, Direct Collocation, Serpentine Tails, Mechatronics

A SYSTEMATIC DESIGN METHODOLOGY FOR ARTICULATED SERPENTINE ROBOTIC TAILS TO ASSIST AGILE ROBOT BEHAVIORS

Isaac Pressgrove

ABSTRACT

In pursuit of producing robots capable of achieving the dexterity exhibited by animals in nature, roboticists have begun to explore the application of robotic tails. This thesis will explore the design, optimization, construction, and implementation of an articulated serpentine robotic tail. Numerous serpentine tail prototypes have been designed and tested; however, they have not yet been integrated with a mobile base. The main challenges preventing the incorporation of serpentine tails with mobile bases include: (1) the large size and inflexible packaging associated with the actuation unit for the tail, (2) the relatively low power to weight ratios of the existing serpentine tail systems, and (3) the complexity of optimizing the tails physical parameters.

Therefore, to address these issues, a novel layout for a serpentine robotic tail actuation unit along with a design optimization methodology for the tail are proposed. The actuation unit will feature a power dense and modular design which allows for flexibility in packaging. Simulation results along with experimental data gathered using a prototype of the design will be reviewed in order to quantify the performance of the actuation unit. Following, a design optimization methodology which uses a modified direct collocation technique will be presented. The optimization allows for the simultaneous optimization of both a trajectory and the physical structure of a tail. Representative results of this technique will be presented and compared against more traditional methods for design optimization.

To conclude the on-going and future work for both the actuation unit and optimization methodology will be stated.

A SYSTEMATIC DESIGN METHODOLOGY FOR ARTICULATED SERPENTINE ROBOTIC TAILS TO ASSIST AGILE ROBOT BEHAVIORS

Isaac Pressgrove

GENERAL AUDIENCE ABSTRACT

Robotic tails largely fall into two categories based on their construction. These two categories are pendulum and serpentine structure. Pendulum structure tails consist of a long rigid rod with a weight attached to the end of it which can be swung to assist in controlling the orientation of the base which it is attached to. Serpentine tails are characterized by their ability to articulate and move in three dimensions similar to cat or monkey tails. The non-rigid structure of the tail opens up many new possibilities for their use. However, these possibilities come at the cost of design complexity. To date this complexity has led to designs for serpentine tails which are too heavy or unwieldy to be easily added to a mobile base. Additionally, the complexity of the tail structure itself make it difficult to optimize the design as has been done previously with pendulum designs.

In an effort to overcome these challenges this thesis presents a novel design for a tail actuation unit and design optimization methodology. The actuation unit design is more power dense and provides greater flexibility in its layout than previous designs. This makes it much easier to adapt to and integrate with a mobile base. This will be demonstrated through the creation of a prototype tailed quadruped featuring the new actuation unit. The optimization methodology will use a technique known as direct collocation which has previously been developed for optimal path planning. This technique accommodates the complexities of serpentine tail designs and allows for the parameters such as length and

weight of the tail to be optimized. The conclusion of the thesis will present the on-going and future work for both the actuation unit and optimization technique.

ACKNOWLEDGEMENTS

I would like to thank Dr. Ben-Tzvi for inviting me to join the Robotics and Mechatronics lab at Virginia Tech. Through this invitation I have met many of the people who have helped to make the completion of this degree possible.

Yujiong Liu, without whose guidance, mentorship, and friendship I would not have made it nearly as far as I have.

Dr. Southward and Dr. Sandu, whose instruction through courses, guidance outside the classroom, and participation as members of my committee have been instrumental in my success as a researcher and member of the Virginia Tech community.

Dr. Asbeck and Dr. Leonessa, whose examples of how to engage with students as instructors and faculty I have and will continue to follow.

The many friends I have made since moving to Blacksburg, who all have helped support me and made this town feel like home.

Without those listed here and many others not specifically named this degree certainly would've been much more difficult if not impossible. Thank you for everything.

The work in the thesis was supported by the National Science Foundation under grant number 1906727.

TABLE OF CONTENTS

LIST OF FIGURES

LIST OF TABLES

1. INTRODUCTION

1.1 Motivation

In nature many animals have tails which are used alongside or in place of other limbs in order to manipulate, propel, maneuver, and/or stabilize [1]. Examples of this include: monkeys using their tails to grasp branches or to balance while walking [2, 3]; kangaroos using their tails as a fifth leg to support and contribute to their unique pentapedal gait [4]; common house cats compensating for disturbances while walking along then beams [5]; and cheetahs using their tails to aid in highspeed turning, acceleration, and deceleration [6]. Seeing the many varied applications of tails in nature have led to researchers taking great interest in applying them towards increasing mobility of mobile robots and comparing them against other forms of inertial reorientation.

The first examples of robotic tail research focused primarily on planar single link pendulum tails as a simplified abstraction of those found in nature. Following the planar pendulums were spatial pendulum tails which allowed for control over an additional degree of freedom as well as use in more some other applications such as self-righting. However, despite the greater range of applications spatial pendulum tails are capable of they are still fairly restricted by their inability to change shape. This prevents the reduction in size of workspace boundary required to perform reorientation task while simultaneously restricting the tail from being able to interact with anything inside of the workspace boundary. This creates an inefficient workspace that makes it difficult to fully utilize the tail in cluttered environments for aid in reorientation. Serpentine tails on the other hand

have the flexibility to change shape allowing them work more effectively in a greater range of environments. Additionally, the ability to change shape allows the tails to access the interior of the workspace. This opens many new useful possibilities such as using the tail as a manipulator appendage with a gripper attached to the end. The possibility of greater and more varied utility has led the most recent research to move away from rigid pendulum tail structures in favor of the more dynamically capable serpentine designs.

Serpentine tails, however, are not without their drawbacks. Primarily they come with significantly increased complexity and all of the added difficulties of integration that come with it. Though several prototypes of serpentine tails have been made already, none have yet been integrated with a mobile base. These prototypes have proven the ability of a serpentine tail to effectively generate inertial loading and proven out different structures for the tail. However, the actuation units have been too large and strict in their layout to be easily integrated with a mobile base. Many of the deficiencies with the actuation units can be addressed through the use of more power dense actuators and a reorganization of those actuators. However, this only addresses the symptoms of brought on by the complexity of serpentine tail systems and leaves the likelihood that the actuation unit will be over built for the needs of the mobile base and tail system as a whole. To ensure that the actuation units are not overbuilt, and the power of the unit is used most effectively, it is necessary to optimize the physical parameters of the tail being driven by the unit. Efforts have been made to optimize the tail designs previously, but they primarily relied on either heuristic methods or only optimized portions of the design.

In order to address both the issues of integration of serpentine tails with mobile bases this thesis will propose a novel actuation unit design and optimization methodology.

The remainder of this chapter will consist of the specific research contributions of this thesis and an outline for the following chapters.

1.2 Contributions

This thesis presents the design and integration of a serpentine robotic tail actuation unit along with a design optimization methodology for the physical parameters of serpentine tails. The serpentine robotic tail is integrated with a reduced complexity quadruped base (RCQ) [7]. The actuators used in the base are experimentally tested and evaluated both on their own and as part of the fully integrated system. The design optimization methodology is formulated using the direct collocation technique in a novel manner that allows for simultaneous generation of an optimal tail trajectory and design to achieve a set goal. The optimization results are presented and compared against more standard techniques using simulation. These works combine to provide the following contributions to the field of robotic tail research:

1. Development of a power dense and modular actuator which enables improvements to the layout of the tail actuation unit
2. A novel layout for a serpentine tail actuation unit which allows for flexible and compact packaging of the actuation unit. This significantly reduces the difficulty of integrating serpentine tails with mobile bases.
3. Redesign of the R3RT-V2 robotic tail to incorporate the new tail actuation unit layout and the power dense modular actuators. This updated tail prototype is then integrated into the RCQ robot in the lab to show the effectiveness of the actuation unit design,.

4. A method to optimize the physical parameters of serpentine robotic tails in conjunction with the optimization trajectories for their motion. This methodology will help guide the design of future tails and better define the necessary effort to drive them.

1.3 Thesis Structure

Chapter 1: Presents motivations of this thesis as well as a list of research contributions.

Chapter 2: Provides a review of existing robotic tails and the methodologies used to design them. Identifies challenges related to the implementation of robotic tails. An analysis of existing design methodologies which have been applied to existing robotic tails is then given. Finally, a design methodology which aims to address the challenges and shortcoming identified in previous work is proposed.

Chapter 3: Presents the development of the tail actuation prototype starting with the design targets. This is followed by the mechanical design of the tail actuation unit and tail subsystems. Results of experiments are then presented

Chapter 4: Presents the chosen design methodology of a modified direct collocation technique. The direct collocation technique is the compared against results from a single shooting optimization as well as results from prior heuristic optimization studies. All results are analyzed using a simulation validated based on experimental data in the previous chapter.

Chapter 5: Provides a summary of the thesis and conclusion based on the presented material along with a statement of future work to be done.

1.4 Selected Publications

Disclosure: Content from these publications were used throughout this thesis.

Conference Papers

I. Pressgrove, Y. Liu and P. Ben-Tzvi, “Design and Implementation of a Power-Dense, Modular, and Compact Serpentine Articulated Robotic Tail”, Proceedings of the 2022 ASME IDETC/CIE, 46th Mechanisms & Robotics Conference, St. Louis, MO, USA, August 14-17, 2022, Accepted.

2. LITERATURE REVIEW

2.1 Robotic Tail Designs

In order to improve upon the design of serpentine tail actuators it is important to understand the history of tail designs and applications. As stated, in the introduction the development of robotic tails began with planar pendulum tails; progressed to spatial pendulum tails; and most recently has been focused on spatial serpentine structures. This section of the literature review will cover notable developments, designs, and applications of first pendulum and then serpentine tails.

2.1.1. Pendulum Tails

For the purposes of this review, pendulum tails will be defined as any tail which consists of a rigid rod connecting a weighted end to a base. According to a literature review conducted by Saab [8] the earliest example of a robotic tail used for inertial reorientation was the Uniroo robot. The Uniroo robot was a single legged hopping robot designed to kinematically replicate a kangaroo. The robot used a planar pendulum tail to control pitch during hopping motion. This control was accomplished by swinging the tail vertically to offset the mass of the leg as it moved through the hopping trajectory [9]. Following Uniroo there was an apparent lack in robotic tail research until Zappa [10], a quasi-passive bipedal robot. Zappa used a single DOF pendulum tail as the only actuated joint on the robot. In order to induce movement of the legs resulting in locomotion Zappa would swing the tail horizontally from side to side. After Zappa there was a significant uptick in robotic tail research. Jusufi et al. modelled a gecko's use of its tail for mid-air reorientation as a two DOF pendulum attached to the body via a universal joint. The model was then verified by

adding a single DOF tail to a quadruped, Stickybot, capable of midair righting along the robot's longitudinal axis [11]. Continuing research based on the findings from the analysis of gecko tails Chang-Siu et al. also tested planar pendulum tails for mid-air inertial reorientation on two other robots. These two are, a four wheeled robot Tailbot [12] and the six legged robot X-RHex Lite [13]. Another example of using a tail for mid-air pitch control include Xiao et al. miniature jumping robot [14]. Research has also been conducted on applications for added stability and control during locomotion. The kangaroo robot designed by Liu et al. utilized a tail to control pitch of the robots body during locomotion [15, 16] while the TAYLRoACH implemented a vertically pinned tail to add yaw position control while running [17]. In a similar vein Patel and Braae added a planar tail in two different configurations to a wheel robot to try and aid in dynamic handling while driving similar to how a cheetah uses their tail while running. The first configuration had the tail pinned to rotate about the vehicles longitudinal axis to improve highspeed cornering [18]. The second rotated the pin 90 degrees so that the tail would aid in pitch control during acceleration and deceleration [19]. A final and unique implementation of planar pendulum tails for inertial reorientation is the climbing robot ROCR developed by Fehlberg et al. which used a tail to induce both quasi-static and dynamic climbing motions [20].

In order to expand the capabilities of a tail to control more than a single DOF it is necessary to move from a design constrained to planar motion to one capable of spatial motion. The following are notable examples of spatial pendulum tails. The first is the addition of a spatial pendulum tail to the MIT Cheetah done by Briggs et al. [21]. This design successfully utilized the tail for disturbance rejection allowing the robot to remaining standing after being impacted by 1.16kg clay mass moving at 5m/s. Another

example is the continuing work of Chang-Siu et al. to expand to a spatial tail for aerial self-righting [22]. This work showed the ability of a tail to correct the orientation of a falling robot from arbitrary positions to a desired landing pose. Continuing progress on the use of spatial tails was made through the development of the Penn Jerboa robot [23-25] and addition of a tail to the Dima II [26]. In addition to furthering the understanding of how tails can be used to aid in locomotion, both of these robots used a unique mounting method. The tails of both were controlled using two co-axial motors to affect change in the pitch and yaw of the tail. This differs from the universal joint synthesized through the use of motors with orthogonal axis used by the other two instances of spatial tails reviewed. This coaxial layout, which is implemented in two distinct ways between the Jerboa and Dima II, provides inspiration for new tail actuation units.

2.1.2. Serpentine Tails

Research conducted with the rigid pendulum tails proved the potential of tails to be used as inertial reorientation devices. However rigid structures still have some short comings, namely, the required workspace and limitations on secondary uses. In order to overcome the drawbacks of rigid pendulum tails and increase overall effectiveness, the latest research has focused on the development of serpentine tails. These tails have greater degrees of freedom allowing for more complex control and flexibility in task implementation.

One of the first serpentine structure tail designs is the DMST [27, 28]. This tail consisted of a chain of cable driven links attached to each other through revolute joints. The first/base link was then mounted to a rotating base. The tail was able to produce an overall bending curvature. The exact shape of the curvature was controlled by the ratio

between pulley diameters that the cable going to each successive link was driven by. This meant that the tail could be made to have a consistent or varying curve along its length. However, this also led to the actuation unit taking up a large volume in order to house the multiple pulleys. A direct descendant of the DMST is the R3RT [29, 30]. This tail followed a similar formula to the DMST, making use of cable driven links attached to each other through revolute joints with a rotating base link. However, unlike the DMST, all links within a given segment of the R3RT are driven by a single pair of antagonistic cables and all links are constrained to have equal bending. This means that each segment of the R3RT (of which there are generally two) have a consistent curvature. The payoff for this reduced complexity is that the actuation unit and tail can both be made more compact.

Another family of serpentine tail designs are those which have segments with combined yaw and pitch motion. These designs are similar to the spatial pendulum tails and distinct from the DMST and R3RT which both featured decoupled rolling and bending. The first of this family is the USRT [31, 32]. Closely related the USRT is the RML tail [33]. Both of these tails use cables to induce bending in segments with elastic backbones. Similar to the R3RT they have consistent bending along a single segment with the ability to add additional segments to increase the overall DOFs of the tail. The compliant nature of both of these tails is both their benefit and drawback. As is often seen discussed in conversations around soft robotics, there are many benefits to compliant systems such as the reduced likelihood of damage to either the robot or its surroundings in the case of a collision. However, the compliance also makes modelling and control of the system much more difficult. The USRT and RML tail do also have the benefit of generally simpler actuation units due to not requiring a method of rotating the base link. A final tail design

that looked to address some of the issues brought on by the compliant backbone of the previous two is the Rigitail [34]. The Rigitail is made up of links connected to each other by a combination of rigid rods and an innovative rigid coupling hybrid mechanism (RCHM). The tail was able to achieve a more rigid structure with similar maneuverability to the other two coupled motion tails. Furthermore, it is able to be fully actuated through the use of just two linear actuators. This tail offers many advantages over prior designs but suffers from two main drawbacks. First the design does not readily provide provisions for introducing a second segment, meaning it would be difficult to expand beyond 2DOF. Second the RCHM is difficult to construct.

2.2 Design Methodologies

Though no comprehensive design methodology has yet been formulated for serpentine tails, there have been many efforts to optimize aspects of their design. This portion of the review will cover design methods and optimization strategies used on both pendulum and serpentine tails to date.

One of the easiest and most common methods is to take a heuristic approach to selecting ideal parameters. In this case, typically a single parameter value is varied at a time and its effect on the system is observed through modelling or simulation outputs. This approach has been used across both pendulum and serpentine tails and usually focuses on two parameter, tail length and tail mass. Research described in [10-12, 17-19] all conducted optimization studies using a heuristic approach with a focus on maximizing the effectiveness of pendulum tails by varying either the tail length, mass, or both. The general result that can be taken from these studies is that increasing the tails moment of inertia up to the point of actuator saturation tends to maximize efficiency. This is valuable as a

starting point for designs. However, it does not give much in the way of specific guidance for designing more complicated serpentine tails which have a more complicated relationship between their length, mass, moment of inertia, and power consumption.

Heuristic approaches are also common with serpentine tails. In [28] Saab looks at how varying the mass and effective curvature of the tail impact the loading it is able to impart on the base. Similar to what was found with pendulum tail, it was found that increasing the mass up to the capacity of the actuators led to increased loading. However, unlike pendulum tails with serpentine tails it was found that the degree of rotation seen by the links also had the ability to increase the tails effectiveness. Liu conducts an optimization study meant to be more generalized to all serpentine tails in [7]. This study uses simulation of a tailed quadruped performing a combined jumping and turning maneuver to investigate the impacts of tail length and mass as ratios of the respective torso measurements. Because this study uses ratios and does not begin with a preset limit for power it's results can be considered more generalized than previous studies. The important results here are to show that even when unbounded by maximum power serpentine tails tend to see a plateau in their performance above a tail to body length ratio of 2 and a tail to body mass ratio of .1.

Some pendulum tail papers such as [21] presented more formal optimizations where derivatives of the dynamic models relating tail parameters to actuation effort could be taken to find unique solutions. However, even these required some assumptions to simplify and linearize the system. The more complicated and highly non-linear dynamics of serpentine tails make this approach infeasible.

2.3 Conclusion

Despite the numerous serpentine tail designs in existence and the simulation work done for nearly every one of them to show their effectiveness in balance and agility of a mobile base, none have yet made it off of the test bench. It is clear then that research needs to pivot from formulating new tail structures to focusing on the integration of an existing tail structure with a mobile base. Therefore, this thesis will present a novel tail actuation unit designed to drive an existing tail structure which can be easily integrated with a mobile base. Furthermore, in an effort to maximize the effectiveness of the actuation unit, this thesis will also propose a design optimization methodology for key parameters of a tails structure.

3. PROTOTYPE DEVELOPMENT AND EXPERIMENTAL RESULTS

3.1 Modeling and Simulation

This section presents the changes to the kinematics of the R3RT tail structure from those used in previous papers. Then the simulation which was used to define the actuation requirements will be described. Finally, the results of simulation will be presented and translated into design requirements.

The kinematics, dynamics, and associated simulation environment used in this paper are based off of those presented in [35]. This paper presents two updates to the kinematic formulation to allow for greater flexibility in investigating design parameters. Those changes are to make the number of links in the tail and location of the center of mass (COM) of the base link variable. Though neither of these changes fundamentally change the kinematics or dynamic modeling of the tail, they do impact overall performance.

The tail, previously composed of 12 links, is now composed of N links split into two planar bending segments composed of $N/2$ links attached to a base link, which provides overall rolling motion. In this way the tail can be said to have 3 DOFs defined by the base link rolling angle α and the two planar bending angles for the links within each planar bending segment, β_1 and β_2. The body fixed frames $\sum J_i \coloneqq (J_i, \mathbf{x}_i, \mathbf{y}_i, \mathbf{z}_i)$, $\sum T \coloneqq (T, \mathbf{x}_0, \mathbf{y}_0, \mathbf{z}_0)$, and $\Sigma P \coloneqq (P, \mathbf{x}_p, \mathbf{y}_p, \mathbf{z}_p)$ for links i through N, the base link, and reduced complexity quadruped (RCQ) base respectively are defined as shown in Fig. 2. It is important to note is that $\sum T$ is located such that $\mathbf{y}_0$ coincides with $\mathbf{y}_p$ and $\mathbf{x}_0$ coincides with

the x-axis of joint 1. The global fixed reference frame is defined as $\Sigma S \coloneqq (S, \mathbf{x}_s, \mathbf{y}_s, \mathbf{z}_s)$. Further detail on modelling can be found in [36].

Important kinematic equations that differ from those described in [36] due to the aforementioned changes to link count and base link COM location are shown below. In these equations, a rotation matrix denoted by ${}^{B}\mathbf{R}_{A}$ is defined as the general rotation from frame ΣA to ΣB. $\mathbf{R}_x$ and $\mathbf{R}_y$ are the principal rotation matrices with respect to x and y axis. Vectors $\mathbf{p}_{0,com}$ and $\mathbf{p}_t$ are defined as the position of the COM of the base link, C_0, and the location of the origin of the base link, T, in ΣS. ${}^{0}\mathbf{p}_{C0}$ is defined as the local vector from T to C_0 in ΣT.

$$ {}^{S}\mathbf{R}_i = \begin{cases} {}^{S}\mathbf{R}_P\mathbf{R}_y(\alpha), i = 0 \\ {}^{S}\mathbf{R}_P\mathbf{R}_y(\alpha)\mathbf{R}_x(i\beta_1), 1 \le i \le \dfrac{N}{2} \\ {}^{S}\mathbf{R}_P\mathbf{R}_y(\alpha)\mathbf{R}_x\left(6\beta_1 + (i - \dfrac{N}{2})\beta_2\right), \dfrac{N}{2} \le i \le N \end{cases} \tag{1} $$

$$ \mathbf{p}_{0,com} = \mathbf{p}_t + {}^{S}\mathbf{R}_0\,{}^{0}\mathbf{p}_{C0} \tag{2} $$

The necessary Jacobians can be obtained by differentiating Eqs. (1) – (2) and factoring out the generalized coordinates. The corresponding Jacobians are listed in Eqs. (3) – (5) where $\mathbf{u}_{m,n}$ is the m dimension unit column vector with 1 on the n-th entry. The tilde over a vector indicates its skew symmetric expansion.1

$$\mathbf{J}_{i,\omega} = \begin{cases} [\mathbf{0}_{3\times3} \quad \mathbf{I}_{3\times3} \quad \mathbf{0}_{3\times3}] + \mathbf{y}_0\mathbf{u}_{9,7}^T, i = 0 \\ \mathbf{J}_{i-1,\omega} + \mathbf{x}_0\mathbf{u}_{9,8}^T, \quad 1 \le i \le \dfrac{N}{2} \\ \mathbf{J}_{i-1,\omega} + \mathbf{x}_0\mathbf{u}_{9,9}^T, \quad \dfrac{N}{2} \le i \le N \end{cases} \tag{3}$$

$$\mathbf{J}_{C0} = -(\widetilde{{}^S\mathbf{R}_0\,{}^0\mathbf{p}_{C0}})\mathbf{J}_{0,\omega} \tag{4}$$

$$\mathbf{J}_{0,com} = \mathbf{J}_t + \mathbf{J}_{C0} \tag{5}$$

Since the changes to the above equations do not directly appear in the equations of motion, the construction of the dynamics is not changed. Details on the dynamic modeling of R3RT system can be found in [35].

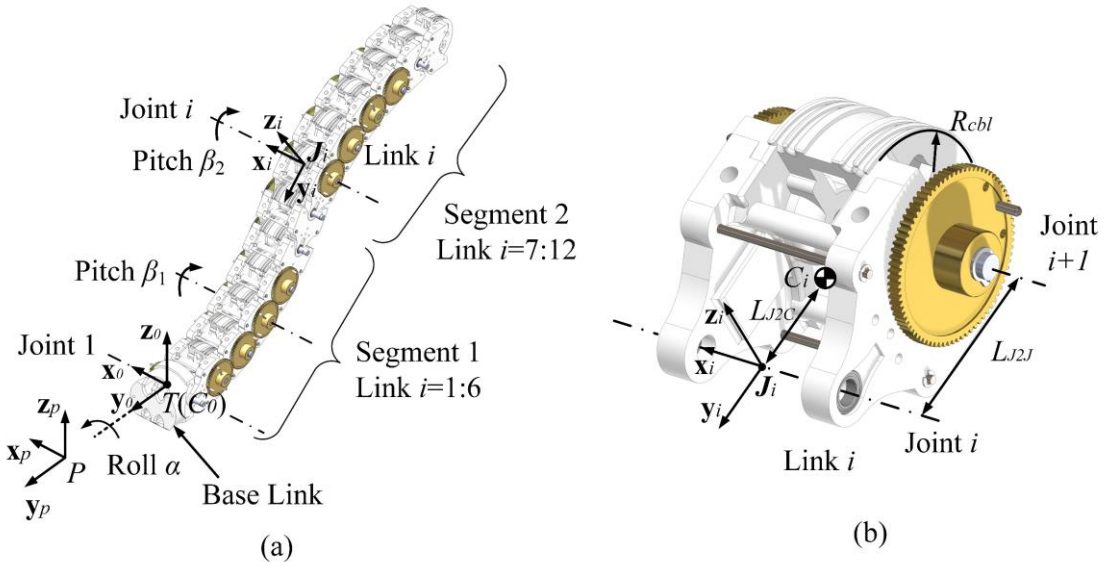

Figure 1 : (a) Kinematic Configuration of The R3RT. (b) Kinematic Configuration for the ith Link

The RCQ was primarily designed to perform maneuvering task as defined and simulated in [35]. Therefore, the design requirements for the tail presented in this paper are

generated using the existing maneuvering simulation with all of the same parameters as set forth in [35] except for the change in number of links and the addition of the new parameter ${}^0\mathbf{p}_{C0}$. When $N = 12$ and ${}^0\mathbf{p}_{C0} = \mathbf{0}$ the simulation is unchanged.

To set a baseline, the optimal tail length of two times the body length and a tail mass of 0.09 times the body mass was used with $N = 12$ and ${}^0\mathbf{p}_{C0} = \mathbf{0}$. The results of this combination showed a peak power of 135W was required, which is consistent with the results in [35]. To add more detail to this requirement, the speed and actuation effort of each DOF were also recorded. The roll actuator effort and velocity are measured in newton-meters and rad/s, respectively. Since the planar bending is driven by cables, the force and velocity for bending are measured in newtons and m/s, respectively. The results are shown in Figure 2. Beyond the baseline, one additional trial was run with the COM of the base link moved to the center of the quadruped (${}^0\mathbf{p}_{C0} = [0 \;\; 0.15 \;\; 0]^T$) and $N = 18$. It was found that these two changes resulted in a much lower peak power requirement of 90 W and correspondingly lower actuator effort and velocity, as shown in Figure 3. Based on

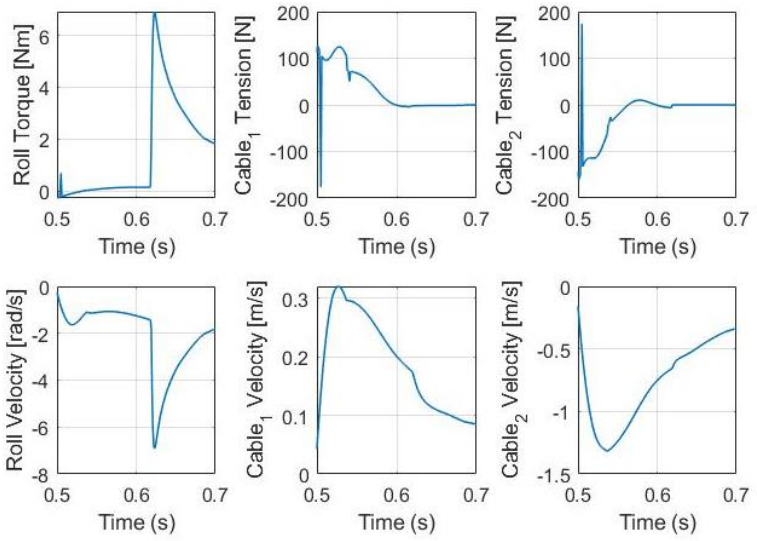

Figure 2 : Actuation Effort and Velocity for Baseline Values

these findings, the design requirements were decided to be as follows: A minimum peak power output of 100 W for all actuators, A roll actuator capable of outputting 9 Nm, bending actuators capable of outputting 150 N, and the ability to have the center of mass of the actuation unit be located in the center of the body.

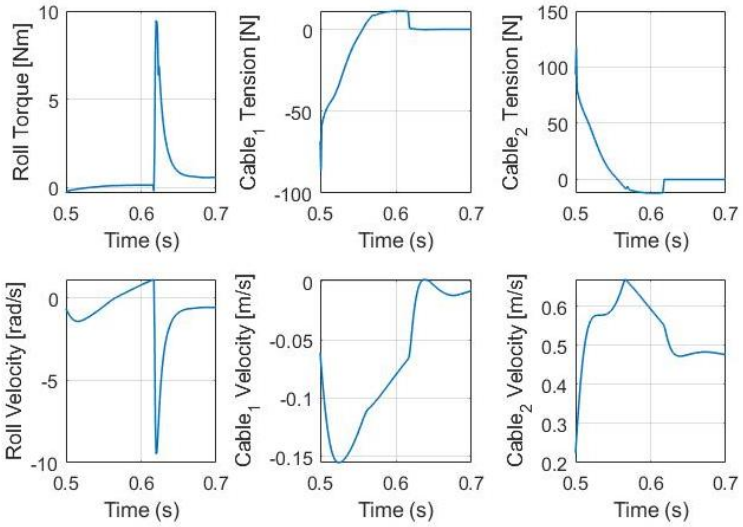

Figure 3 : 18-Link Tail with Repositioned Base Link COM

3.2 Mechanical Design

This section details the mechanical design of the tail actuation architecture and how it meets the design requirements from the previous section while improving upon prior designs.

As noted previously, one of the largest obstacles to integrating an articulated tail with a mobile base is the mass of the actuation unit. In simulation the base link represents the actuation unit. Since the dynamic targets were set using the predicted 6 kg RCQ model from [30], this iteration aims for an actuation unit totaling a mass of no more than 1 kg.

Also identified as an obstacle to integrating existing articulated tail designs with a mobile base is the relatively large size and bulky fixed shape. This causes two main issues. First, it is difficult to package the actuation units in a compact chassis with other critical components. Second, it significantly limits flexibility in locating the center of mass of the mobile base, which is heavily influenced by the mass of the tail actuation unit. To remedy these issues, the tail actuation architecture presented will be modular, thereby allowing for varying distances between the roll actuator, bending actuators, tensioner, and tail base.

3.2.1. Actuator Design

The first step to achieving the dynamic targets, total mass, and flexible packaging goals is to design a compact and power dense actuator. To do this, inspiration was taken from the actuator designed for the MIT Cheetah robot series. Their actuator features a brushless pancake style out runner motor attached to a planetary gearbox with an onboard motor controller board [37]. This style of actuator provides a lightweight compact package capable of a relatively high peak torque output. These attributes make the layout well suited for driving the quick but highly dynamic movements of a robotic tail.

In order to minimize packaging space requirements, the tail actuator must be as compact as possible. This is especially true for the planar bending actuators, which need to be able to rotate with the tail in order to avoid complicated cable routings. Because of this, the RCQ torso width of 200 mm minus an additional 50 mm to account for other

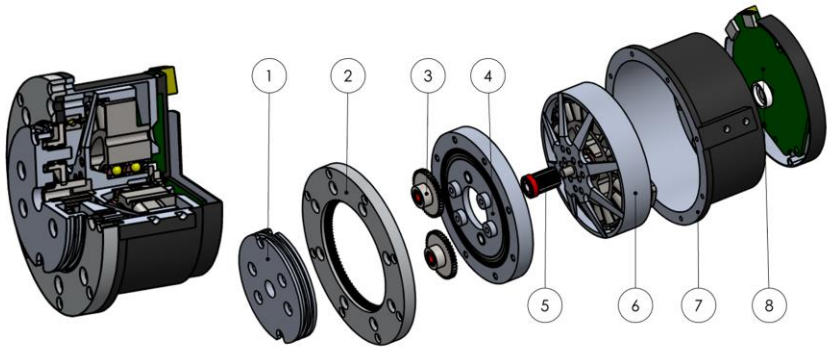

1 Actuator Output
2 Ring Gear
3 Planets
4 Planet Carrier
5 Sun
6 T-Motor MN6007
7 Back Housing
8 Controller

Figure 4 : Exploded View of The Actuator

components that may be needed was considered to be the limit of the packaging for the bending actuators. In order to meet the modular requirement, it was decided that the actuator developed should be able to drive any of the DOFs with little or no modifications. These, in combination with the power and peak torque requirements from the previous

section, make up the complete set of requirements for the actuators.

For motor selection, it was found that the T-Motor MN6007 proved to be an attractive option due to its reported peak power of 936 W, peak torque of 1.3 Nm, and relatively small outer diameter of 67 mm. To bring the torque output up to meet the design

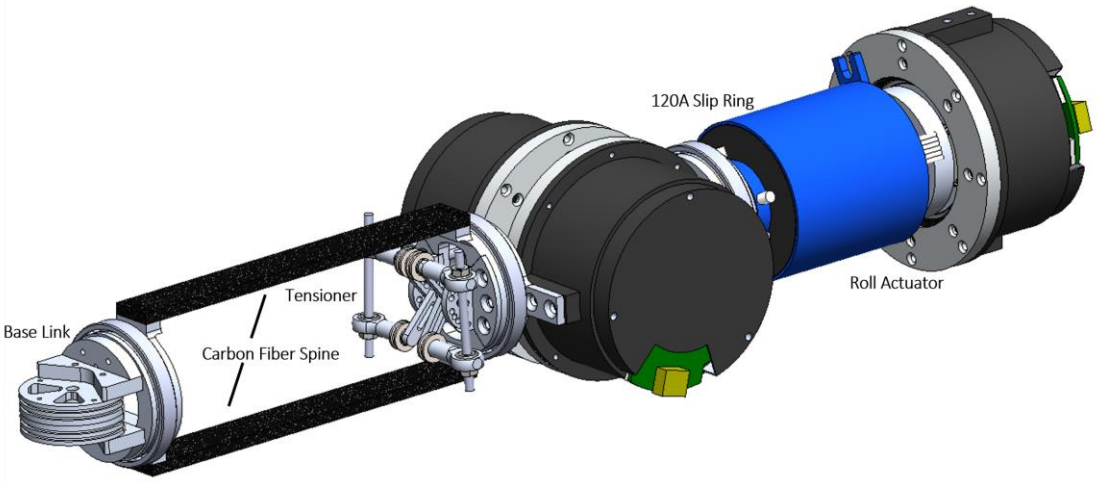

Figure 5 : Tail Actuation Unit Assembly

requirement of 9 Nm, the actuator would need a gear reduction of at least 7. Based on available gears, it was decided that a single stage planetary reduction of 7.25 would be used. To meet the linear force output requirement, the pulleys driving the planar bending would need to have a radius no larger than 63 mm.

Error! Reference source not found. shows an exploded view of the final actuator d esign. The actuator has an outer diameter of 82 mm and axial length of 53 mm. The actuator design includes a built-in pulley with a radius of 23.5 mm as part of the planet carrier which is included in the 53 mm axial length. This means that when paired together, as shown in

Fig. 6, with 0.5 mm clearance between them, the total axial length is only 106.5 mm with a maximum edge to edge dimension of 125 mm across the diagonal.

The actuator has a mass of 460 g, which would violate the design requirement set for the mass of actuation unit if all three actuators rotated as they did in the previous R3RT design. However, because the roll actuator is now fixed to the chassis and does contribute to the rotating mass, it can be considered part of the body. More detail on the total mass of the actuation unit and layout will be given in section 3.3.

The final product of this design is a single 900 W actuator with a mass of only 460 g, which can be used for all three DOFs. The actuator provides a predicted peak torque of 9 Nm and peak pulling force of 380 N and has a power density of 1.95 W/g.

3.2.2. Tensioning System

A compact, reliable, and easily adjustable tensioner is crucial to the proper operation of the tail. In testing the original R3RT tail design, it was found that the lack of a reliable tensioner made control of the bending DOFs more difficult and in some extreme cases caused complete failure by allowing the cable to jump off the pulley.

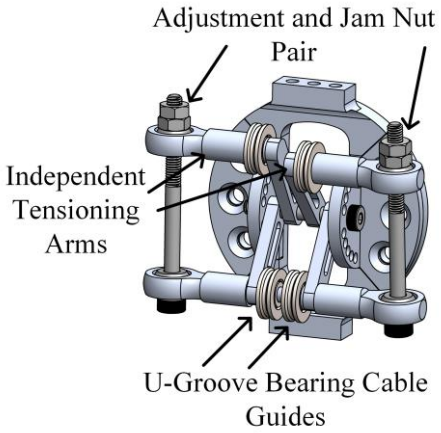

Figure 6 : Tensioner Mechanism

For the tensioner to be considered reliable, it must resist loosening when repeatedly exposed to shock loading. To ensure that the tensioner for this tail design does not loosen, it is tightened by tightening an adjustment nut on a bolt, which is then secured with a jam nut. This way not only is the jam nut prevent the adjustment from backing off, but the force applied against the adjustment method is guaranteed not to be in a direction which could rotate the nut.

3.2.3. Actuation Unit Layout and Integration with Mobile Base

The actuators take care of the design requirements except for one. That is the need for the COM of the actuation unit to be located as close as possible to the center of the mobile base. As was shown in [32], the location of the system COM has a large impact on the ability of the robot to successfully complete a maneuvering task. It is therefore advantageous to be able to have flexibility in locating the actuation unit COM. For the RCQ layout, it was decided that keeping the actuation COM as close to the geometric center of the robot would be best, but in other applications it may be preferential to have the COM be located elsewhere. In order to provide this flexibility, the actuation unit presented here has a modular design split into three main components connected by a rigid spine. As shown in Fig. 5, these three components are the base link, planar bending actuator pair, and roll actuator. In this iteration, the tensioner is paired with the planar bending actuators, but it could just as easily be paired with the base link if this was preferred. The Roll actuator and planar bending pair are connected via a 12 mm rod which passes through the 120 A slip ring and transmits the rolling motion. The planar bending pair is then connected to the base link via a pair of carbon fiber plates, which are spaced apart to provide maximum torsional stiffness without compromising packaging space within the RCQ chassis.

The combination of the power dense actuators which provide nearly 2 W/g, compact and reliable tensioner mechanism, and unique modular layout make this actuation module easy to integrate with a mobile robotic base. To give context to the scale of improvement made by this design, it will be compared against the original R3RT. The original design used three Maxon EC-i40 motors. The total mass of actuation module is 6.4 kg giving it a combined power density of 0.047 kW/kg. The total mass of the new actuation unit is a full quarter of the previous at 1.6 kg giving it an overall peak power density of 1.7 kW/kg. The T-Motor does not provide a clear continuous power rating but taking the standard estimation of continuous power being one fourth of the peak, the new actuation module would have a power density of 0.425 kW/kg. This is a tenfold improvement over the existing R3RT design. Additionally, since the roll actuator is fixed to the chassis and non-rotating in this new design, it can be considered part of the chassis rather than actuator, as it is in the existing design. This helps to reduce rolling torque requirements and overall power draw of the system. This means that in simulation the actuation unit will only be considered to have a mass of 1.14 kg. Calculations for the moment of inertia will also exclude the roll actuator. As well as being only one fourth the mass and ten times more power dense than the original R3RT, the modular layout significantly improves ease of packaging and integration. This is poignantly displayed in Fig. 8 where the new design can be seen neatly packaged into the base to fit around other actuators and the battery pack with additional space for controller boards left open.

The increased power density, lower weight, and flexible layout will make integrating a tail and mobile base significantly easier in the future. This will facilitate the movement of future research into the performance and applications of articulated serpentine tails out of simulation and into real world testing.

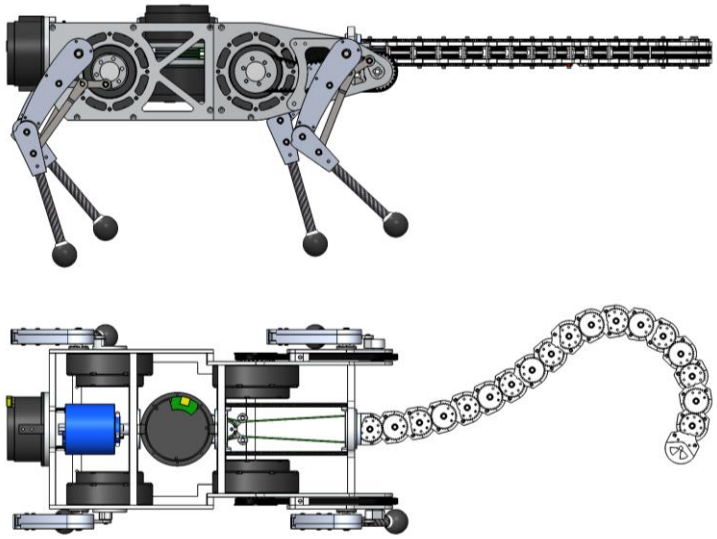

Figure 7 : Finalized CAD Model of R3RT-V2 Integrated with RCQt

3.3 Experiments

3.3.1. Actuator Testing

To verify the performance of the new design before physical prototypes were manufactured, two additional simulations were conducted. The first simulation used the same parameters for the base and 18-link tail as before, but substituted in values for the mass, moment of inertia, and COM location of the new actuation unit as well as updated saturation limits based on the new actuators. This simulation showed a peak power requirement of 95.6 W, a peak rolling torque of 9 Nm, and a peak cable tension of 90 N. This confirmed that the previously set power and actuation effort targets were still valid.

The slightly higher values from this simulation versus the original can likely be explained by the slight increase of mass in the effective base link from 1 kg to 1.14 kg. The second simulation brought the full model up to date with the finalized CAD for both the RCQ base and 18-link tail by updating all masses, moments of inertia, link lengths, and COM locations to match the CAD. This simulation again verified design targets as well as gave a more thorough comparison of how well the integrated design met design goals beyond just comparing values against the previously set targets. The values used for this final simulation are listed in Table 1 and plots of the actuator effort and velocity can be seen in Fig 9. With all values were updated to match the finalized CAD, the simulation predicted a peak power requirement of only 63.7 W, a peak rolling torque of 8 Nm, and a peak cable tension of 85 N. These results give a high degree of confidence that the targets set earlier will be sufficient.

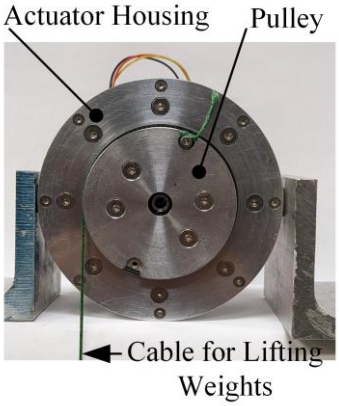

Figure 8 : Actuator Prototype

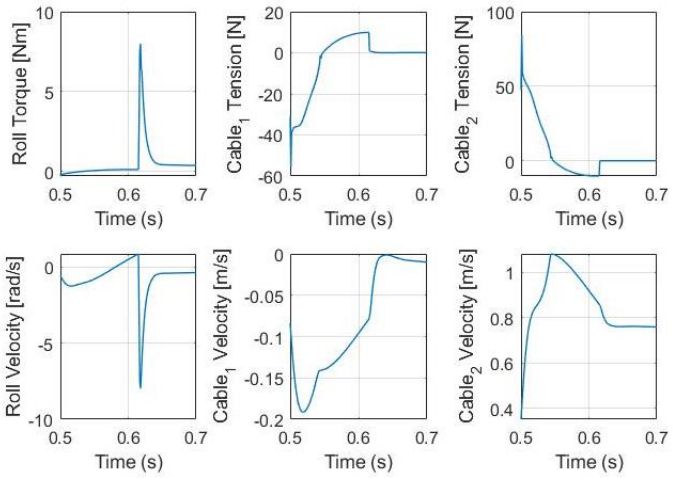

Figure 9 : Simulation Results with Values from Finalized CAD

Two initial experiments were conducted to test the performance of the actuators. The first experiment tested the peak torque output of the actuator and the second looked at the power efficiency. For both experiments, the actuator was powered by a 900 W power supply set to supply a constant 24 volts.

The first experiment was conducted by tying weights of increasing mass to the end of a cable wrapped around the actuator pulley (shown in Fig. 8) and commanding a 5 rad/s rotation. This experiment yielded several important conclusions. First, the actuator is capable of lifting 15 kg at a max angular speed of 4.23 rad/s, corresponding to an output of 147 N cable tension and 3.45 Nm of torque while only drawing 2.6 amps. Second, the PID controller currently programmed into the motor controller board has significant steady state error and was struggling to reach the commanded speed under any given load. Third, there is an issue with voltage spikes during initial startup of the actuator when attempting to lift higher loads leading to shorting out of the controller board protection circuit. The first piece of information is very promising since it shows that the actuator can nearly meet the cable

tension requirement as is and is over a third of the way to the torque requirement while drawing less than a tenth of the motors rated peak current of 40 amps. Once the issues with the controller are resolved and the actuator is able to draw full current, there should be no issue meeting the full design requirements.

The second actuator test looked into the efficiency of the actuator under different loads at a range of speeds. For this experiment the actuator was made to lift a 5, 10, and 15 kg mass at commanded speeds of 5, 7, and 9 rad/s. The power in based on current draw at

Table 1 : CAD Model Properties Used in Simulation

Property Name	Value
Base Link Mass [kg]	1.14
Base Link MOI $[kg \cdot m^2]$	$diag([5.57\ 1.05\ 5.18]) \times 10^{-3}$
Tail Link Mass [kg]	0.023
Tail Link MOI $[kg \cdot m^2]$	$diag([4.98\ 3.69\ 6.14]) \times 10^{-6}$
RCQ Base Mass [kg]	5.93
RCQ MOI $[kg \cdot m^2]$	$diag([8.23\ 6.49\ 13.08]) \times 10^{-2}$

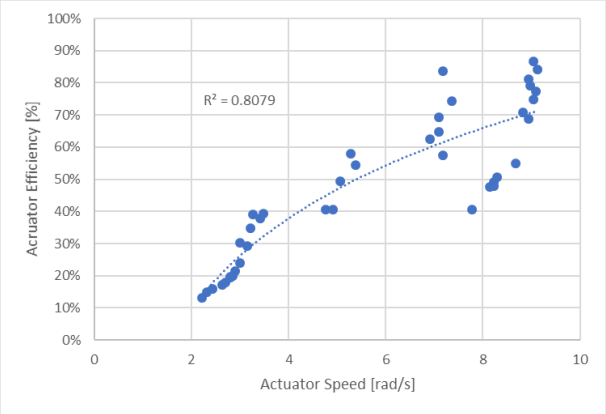

Figure 10 : Actuator Efficiency vs. Speed

a fixed voltage was then compared against the power out calculated as $torque \times speed$. As can be seen in Fig. 11, the efficiency follows a roughly logarithmic trend increasing to be close to 70% efficient at higher speeds. This information is important to quantifying the performance of the gearbox in the actuator design. According to the MN6007 data sheet, the motor has an average efficiency of 78% at speeds from 289 rad/s to 547 rad/s. Based on this and the apparent flattening of the efficiency curve in the data show in Fig. 11 at around 9 rad/s actuator output speed (65 rad/s motor speed), a rough estimate for the actuator efficiency can be obtained. To do this, the average efficiency for speeds above 8 rad/s is obtained and divided by the average 78% efficiency of the MN6007. The average efficiency above 8 rad/s is 65%, which yields a gearbox efficiency of 83.8%. This is low for a single stage planetary gearbox, which would normally be expected to perform above 90% efficiency but given that the number of data points used is small and relatively spread out, and the data is taken well below the efficient range for the motor, it can be considered a good initial result.

The simulation results found using the most accurate values currently available, combined with promising initial experiments with a prototype actuator, give a high level of confidence that the full prototype of the tail actuation module will perform all desired task without issues.

3.3.2. Full System Testing

In order to further validate the actuation unit a full system jumping yaw maneuver test was performed. For this experiment the tail was held flat, and the first segment was swung through its full range of motion while the mobile base was in the air following a vertical jump. This experiment closely resembles the simulations conducted which were

used to set the design requirements. In addition to validating the performance of the actuation unit this experiment also allows for the simulation to be correlated with real world data. This correlation is important as the simulation will be used to analyze optimization results discussed in the next chapter.

The mobile base used for this experiment is a modified version of the RCQ which will be referred to from here on out as the RCQt. This platform uses the same leg design as is covered in [7]. However, the body is modified slightly to accommodate the actuation unit. Figure 7 shows the CAD of the RCQt. The important physical parameters of the RCQt are summarized in Table 2. The RCQt prototype was equipped with an IMU which recorded the roll, pitch, and yaw throughout the experiment at 40Hz.

Table 2: Experimental Setup Properties Used in Simulation

Property Name	Value
Base Link Mass [kg]	1.16
Base Link MOI [$kg \cdot m^2$]	$diag([5.096\ 1.058\ 5.484]) \times 10^{-3}$
Tail Link Mass [kg]	0.046
Tail Link MOI [$kg \cdot m^2$]	$diag([12.58\ 10.48\ 14.93]) \times 10^{-6}$
RCQ Base Mass [kg]	5.39
RCQ MOI [$kg \cdot m^2$]	$diag([7.657\ 3.103\ 9.220]) \times 10^{-2}$

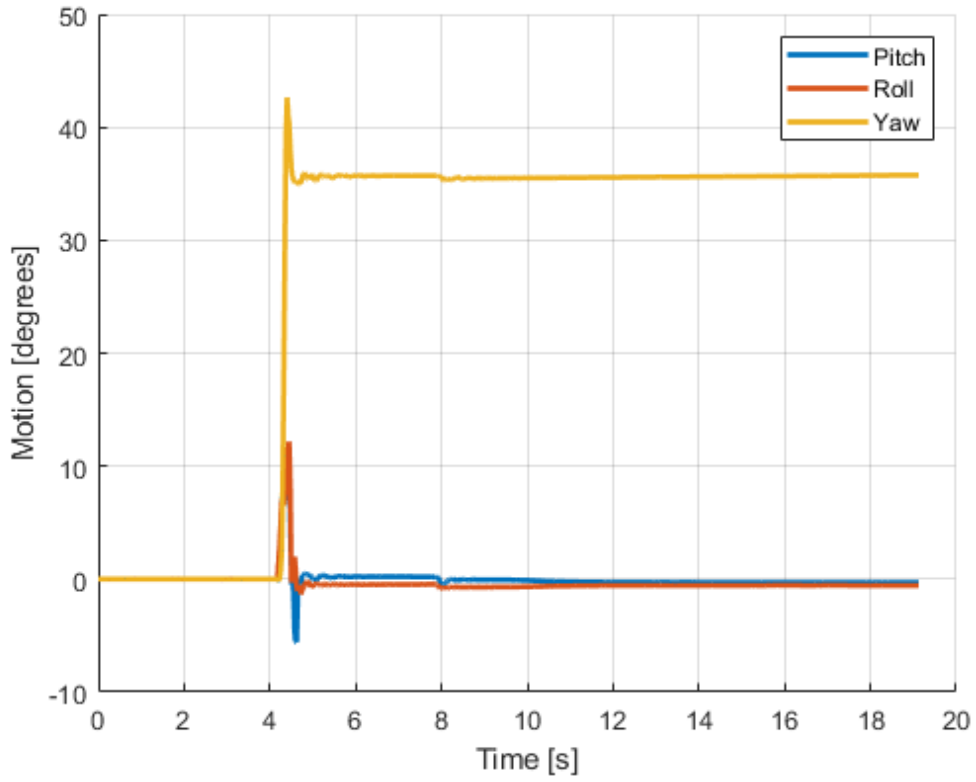

Figure 11 : IMU Data from Yaw Maneuver Experiment

The RCQt was equipped with a 2-segment tail for this experiment. The important physical parameters of the tail can be found in Table 2. The maneuver consisted of swinging the tail through the first segments full range of motion corresponding to a β_1 of $\frac{-\pi}{14}\ to\ \frac{\pi}{14}$ with $\beta_2\ and\ \alpha$ being held at constant values of 0 and $\frac{\pi}{2}$ respectively. The change in angle of β_1 was given as a step input while the robot was in the air. Review of the video footage shows that the actual tail swing lasted .25ms. The roll, pitch, and yaw values recorded by the IMU can be seen in Figure 11. The important result from this experiment is that without any optimization of the tail or its trajectory the RCQt is able to achieve a change in yaw of 42° which then stabilized to 35°. From the video footage taken it can be seen that the overshoot and settling is caused by the tail impacting the side of the base and

turning it back slightly before landing. This exceeds the expected performance since the torque and power requirements were set based on attempting a 30° rotation as discussed in [7].

The experimental data was also used to validate a floating base simulation model used described by Eqns.6-26. The simulation was updated to match prototype physical parameters. Then made to follow the experimental tail trajectory interpreted a set of cubic splines generated using the MATLAB pchip function. As can be seen in Figure 12 the partial feedback linearization controller tracks the given trajectory well. Figure 13 shows that the simulation produces similar yaw motion to that observed during the simulation.

$$ {}^{S}\mathbf{R}_{i} = \begin{cases} {}^{S}\mathbf{R}_{P}\mathbf{R}_{y}(\alpha), \; i = 0 \\ {}^{S}\mathbf{R}_{P}\mathbf{R}_{y}(\alpha)\mathbf{R}_{x}(i\beta_1), \;\; 1 \le i \le S_1 \\ {}^{S}\mathbf{R}_{P}\mathbf{R}_{y}(\alpha)\mathbf{R}_{x}(S_1\beta_1 + (i - S_1)\beta_2), \; S_1 < i \le N \end{cases} \tag{6} $$

$$ \mathbf{p}_{t} = \mathbf{P} - L_{p2t}\mathbf{y}_0 \tag{7} $$

$$ \mathbf{p}_{i,jnt} = \begin{cases} \mathbf{p}_{t}, \; i = 1 \\ \mathbf{p}_{i-1} + \mathbf{p}_{i-1,j2j}, \; i > 1 \end{cases}; \quad \begin{cases} \mathbf{p}_{i,j2c} = -L_{j2c}\mathbf{y}_{i} \\ \mathbf{p}_{i,j2j} = -L_{j2j}\mathbf{y}_{i} \end{cases} \tag{8} $$

$$ \mathbf{p}_{i,com} = \mathbf{p}_{i,jnt} + \mathbf{p}_{i,j2c} \tag{9} $$

$$ \boldsymbol{\omega}_{i} = \begin{cases} \boldsymbol{\omega} + \dot{\alpha}\mathbf{y}_0, \; i = 0 \\ \boldsymbol{\omega}_{i-1} + \dot{\beta}_1\mathbf{x}_0, \;\; 1 \le i \le S_1 \\ \boldsymbol{\omega}_{i-1} + \dot{\beta}_2\mathbf{x}_0, \;\; S_1 < i \le N \end{cases} \tag{10} $$

$$ \mathbf{v}_{t} = \mathbf{v} + \boldsymbol{\omega} \times \mathbf{p}_{t} \tag{11} $$

$$ \mathbf{v}_{i,jnt} = \begin{cases} \mathbf{v}_{t}, \; i = 1 \\ \mathbf{v}_{i-1} + \mathbf{v}_{i-1,j2j}, \; i > 1 \end{cases}; \quad \begin{cases} \mathbf{v}_{i,j2c} = \boldsymbol{\omega}_{i} \times \mathbf{p}_{i,j2c} \\ \mathbf{v}_{i,j2j} = \boldsymbol{\omega}_{i} \times \mathbf{p}_{i,j2j} \end{cases} \tag{12} $$

$$ \mathbf{v}_{i,com} = \mathbf{v}_{i,jnt} + \mathbf{v}_{i,j2c} \tag{13} $$

$$\dot{\omega} = \begin{cases} \dot{\boldsymbol{\omega}} + \ddot{\alpha}\mathbf{y}_0 + \dot{\alpha}\boldsymbol{\omega}_0 \times \mathbf{y}_0, \ \mathrm{i} = 0 \\ \dot{\boldsymbol{\omega}}_{\mathrm{i}-1} + \ddot{\beta}_1\mathbf{x}_0 + \dot{\beta}_1\boldsymbol{\omega}_0 \times \mathbf{x}_0, \quad 1 \le \mathrm{i} \le \mathrm{S}_1 \\ \dot{\boldsymbol{\omega}}_{\mathrm{i}-1} + \ddot{\beta}_2\mathbf{x}_0 + \dot{\beta}_2\boldsymbol{\omega}_0 \times \mathbf{x}_0, \quad \mathrm{S}_1 < \mathrm{i} \le \mathrm{N} \end{cases} \tag{14}$$

$$\dot{\mathbf{v}}_{\mathrm{t}} = \dot{\mathbf{v}} + \tilde{\dot{\boldsymbol{\omega}}}\,\mathbf{p}_{\mathrm{t}} + \tilde{\boldsymbol{\omega}}^{\mathbf{2}}\mathbf{p}_{\mathrm{t}} \tag{15}$$

$$\dot{\mathbf{v}}_{\mathrm{i,jnt}} = \begin{cases} \dot{\mathbf{v}}_{\mathrm{t}}, \ \mathrm{i} = 1 \\ \dot{\mathbf{v}}_{\mathrm{i}-1,\mathrm{jnt}} + \dot{\mathbf{v}}_{\mathrm{i}-1,\mathrm{j2j}}, \ \mathrm{i} > 1 \end{cases}; \quad \begin{cases} \dot{\mathbf{v}}_{\mathrm{i,j2c}} = \tilde{\dot{\boldsymbol{\omega}}}\,\mathbf{p}_{\mathrm{i,j2c}} + \tilde{\boldsymbol{\omega}}^{\mathbf{2}}\mathbf{p}_{\mathrm{i,j2c}} \\ \dot{\mathbf{v}}_{\mathrm{i,j2j}} = \tilde{\dot{\boldsymbol{\omega}}}\,\mathbf{p}_{\mathrm{i,j2j}} + \tilde{\boldsymbol{\omega}}^{\mathbf{2}}\mathbf{p}_{\mathrm{i,j2j}} \end{cases} \tag{16}$$

$$\dot{\mathbf{v}}_{\mathrm{i,com}} = \dot{\mathbf{v}}_{\mathrm{i,jnt}} + \dot{\mathbf{v}}_{\mathrm{i,j2c}} \tag{17}$$

$$\mathbf{J}_{\mathrm{b},\omega} = [\mathbf{0}_{3\times3} \quad \mathbf{I}_{3\times3} \quad \mathbf{0}_{3\times3}] \tag{18}$$

$$\mathbf{J}_{\mathrm{b,x}} = [\mathbf{I}_{3\times3} \quad \mathbf{0}_{3\times3} \quad \mathbf{0}_{3\times3}] \tag{19}$$

$$\mathbf{J}_{\mathrm{i},\omega} = \begin{cases} [\mathbf{0}_{3\times3} \quad \mathbf{I}_{3\times3} \quad \mathbf{0}_{3\times3}] + \mathbf{y}_0\mathbf{u}_{9,7}^{\mathrm{T}}, \ \mathrm{i} = 0 \\ \mathbf{J}_{\mathrm{i}-1,\omega} + \mathbf{x}_0\mathbf{u}_{9,8}^{\mathrm{T}}, \quad 1 \le \mathrm{i} \le \mathrm{S}_1 \\ \mathbf{J}_{\mathrm{i}-1,\omega} + \mathbf{x}_0\mathbf{u}_{9,9}^{\mathrm{T}}, \quad \mathrm{S}_1 < \mathrm{i} \le \mathrm{N} \end{cases} \tag{20}$$

$$\mathbf{J}_{\mathrm{i,com}} = \mathbf{J}_{\mathrm{i,jnt}} + \mathbf{J}_{\mathrm{i,j2c}} \tag{21}$$

$$\mathbf{J}_{\mathrm{i,jnt}} = \begin{cases} [\mathbf{I}_{3\times3} \quad -\tilde{\mathbf{p}}_{\mathrm{t}} \quad \mathbf{0}_{3\times3}], \ \mathrm{i} = 1 \\ \mathbf{J}_{\mathrm{i}-1} + \mathbf{J}_{\mathrm{i}-1,\mathrm{j2j}}, \ \mathrm{i} > 1 \end{cases}; \quad \begin{cases} \mathbf{J}_{\mathrm{i,j2c}} = -\tilde{\mathbf{p}}_{\mathrm{j2c}}\mathbf{J}_{\mathrm{i},\omega} \\ \mathbf{J}_{\mathrm{i,j2j}} = -\tilde{\mathbf{p}}_{\mathrm{j2j}}\mathbf{J}_{\mathrm{i},\omega} \end{cases} \tag{22}$$

$$\mathbf{J}_{\mathrm{ta}} = [\mathbf{0}_{3\times6} \quad \mathbf{I}_{3\times3}] \tag{23}$$

$$\mathbf{H}\ddot{\mathbf{q}} = \mathbf{J}_{\mathrm{ta}}^{T}\boldsymbol{\tau}_{\mathrm{ta}} - \mathbf{C}(\mathbf{q}, \dot{\mathbf{q}}) \tag{24}$$

$$\boldsymbol{\tau}_{\mathrm{ta}} = [\tau_{\alpha} \quad \mathrm{S}_1\mathrm{R}_{\mathrm{cbl}}\mathrm{T}_1 \quad \mathrm{S}_2\mathrm{R}_{\mathrm{cbl}}\mathrm{T}_2]^{\mathbf{T}} \tag{25}$$

$$\mathbf{H} = \mathrm{m}_{\mathrm{b}}\mathbf{J}_{\mathrm{b,x}}^{\mathrm{T}}\mathbf{J}_{\mathrm{b,x}} + \mathbf{J}_{\mathrm{b},\omega}^{\mathrm{T}}\mathbf{I}_{\mathrm{b}}\mathbf{J}_{\mathrm{b},\omega} \sum_{\mathrm{i}=1}^{\mathrm{N}} \mathrm{m}_{\mathrm{link}}\mathbf{J}_{\mathrm{i,com}}^{\mathrm{T}}\mathbf{J}_{\mathrm{i,com}} + \mathbf{J}_{\mathrm{i},\omega}^{\mathrm{T}}\mathbf{I}_{\mathrm{i,tail}}\mathbf{J}_{\mathrm{i},\omega} \tag{26}$$

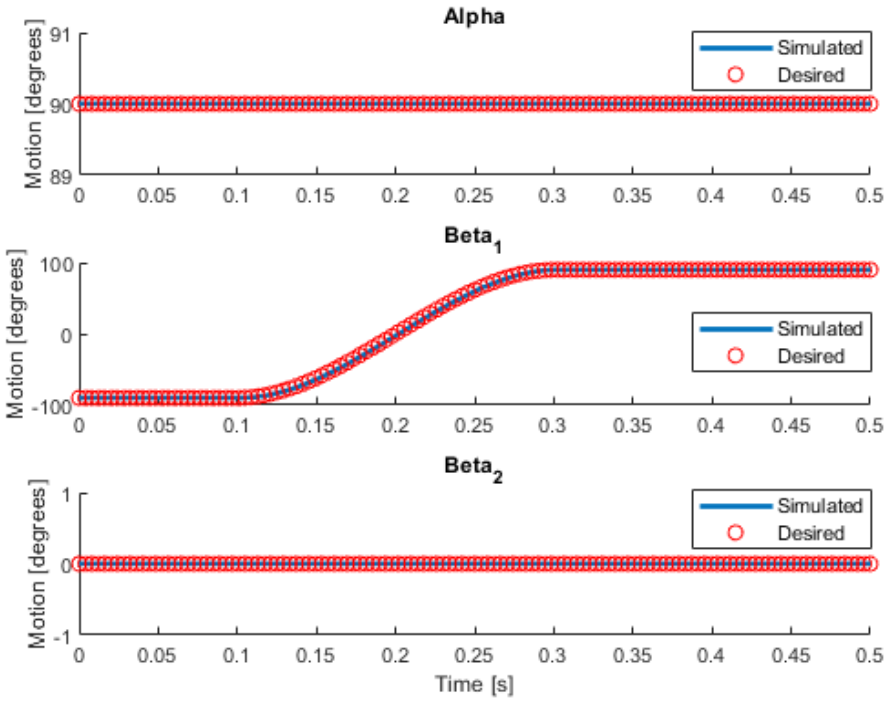

Figure 12 : Experimental Tail Trajectory Tracking

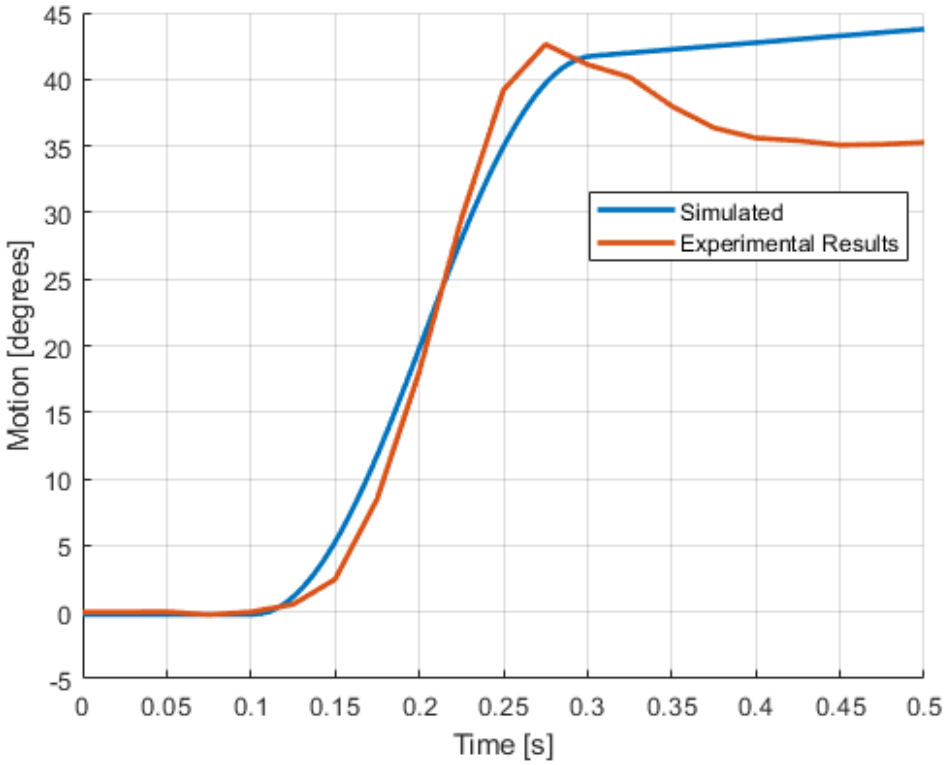

Figure 13 : Experimental vs. Simulated Yaw Motion

4. DESIGN OPTIMIZAITON FORMULATION

4.1 Problem Definition

Up till this point the only optimal design studies have been conducted for serpentine robotic tails. These studies have taken a heuristic approach to determining what range of parameters constitute an optimal design. These have been useful in setting up design guidelines and increasing understanding of how different tail parameters impact the effectiveness of the system. However, they cannot be counted as comprehensive design optimization methods. This is because their methods cannot be generalized to new designs, scenarios, or objective functions. Any change in the setup of the study would require for the whole method to be reworked around the new scenario. Then an array of parameter values would have to be run through anew in order to understand how the new system responds. Therefore, a new comprehensive method is proposed. The new method seeks to create a framework for the optimization that new tail models, use cases, and objectives can be slotted into without need to rework other parts of the method. To do this the new method will use a modified version of the direct collocation trajectory optimization technique. This modified version will allow the optimization to not only generate an optimal trajectory for the tail, but also simultaneously select optimal tail parameters to match the trajectory.

4.2 Direct Collocation Method

Direct collocation is a numerical optimization technique typically used for trajectory generation. The technique relies on cutting up the duration of an event into a number of decision points, typically referred to as knot points. At each of these decision points the optimization problem is given the states of a system. The relationship between

states of the system at different time steps are then imposed as constraints between points formulated as numerical integrations of the dynamics. The formulation in this paper will focus on the use of trapezoidal quadrature rule, but the method presented would work with any other reasonable selection such as the Hermite-Simpson quadrature rule.

In order to use the direct collocation method to find both an optimal path as well as optimal tail parameters a modification must be made from the standard formulation. As mentioned, the decision variables at each knot point would typically consist of the states of the system and control inputs. To accommodate the tail parameters additional decision variables must be added to every knot point. However only the new tail parameter decision variables in the first knot point will be unconstrained. All new tail parameter decision variables after the first knot point will be constrained to be equal to those chosen for the first knot point. This formulation is shown in Eqs. 26-35 below which are based off of [38]. These equations follow the notation laid out in Table 3.

Table 3 : Notation for Direct Collocation

Variable	Description
t_k	Time at knot point
N_k	Number of trajectory segments
h_k	Duration of segment k
x_k	State at knot point k
u_k	Control at knot point k
w_k	Integrand of objective function at point k
f_k	System dynamics at point k
q	Generalized coordinates of robotic system
s_k	Static or time invariant parameters
d_k	All decision variable at point k

$$\mathrm{q} = [\Phi_X, \Phi_Y, \Phi_Z, \alpha, \beta]^T \tag{26}$$

$$x_k = \begin{bmatrix} q \\ \dot{q} \end{bmatrix} \tag{27}$$

$$u_k = [\tau_\alpha, \tau_\beta]^T \tag{28}$$

$$s_1 = \begin{bmatrix} c_i \\ \vdots \\ c_N \end{bmatrix} \; and \; s_2 \rightarrow s_N \equiv s_1 \tag{29}$$

$$d_k = \begin{bmatrix} s_k \\ x_k \\ u_k \end{bmatrix} \tag{30}$$

$$\ddot{q} = M^{-1}(F - C(q, \dot{q}) - G(q)) \tag{31}$$

$$f_k = \dot{x} = \begin{bmatrix} \dot{q} \\ \ddot{q} \end{bmatrix} \tag{32}$$

$$x_{k+1} - x_k - (\frac{1}{2}(h_k)(f_{k+1} + f_k)) = 0 \tag{33}$$

$$\min_{u(t)} \int_{t_0}^{t_{N_k}} w(\tau)\, d\tau \approx \min_{w_k} \sum_{k=0}^{N-1} \frac{1}{2}(h_k)(w_k + w_{k+1}) \tag{34}$$

$$\min_{x_N} g(x_n) \tag{35}$$

This general setup allows for the addition of time invariant parameters to the traditional direct collocation method. For the purposes of this thesis, only link length and link mass parameters will be added as new time invariant decision variables. With the addition of these new variables both the tail trajectory and physical parameters can be simultaneously optimized. This allows for a more generally optimal set of tail parameters to be selected than using a single shooting optimization or heuristic optimization method would result in.

Eqs. 29 and 33 enforce the time invariance of the link length/mass and system dynamics respectively. Eq. 34 is the path objective function while Eq. 35 is a boundary objective, meaning the optimization completed for this example is in Bolza form. Additional path and boundary constraints can be added to the problem as will be discussed in the results section.

In order to reduce computational time, the direct collocation method was setup to use a simplified version of the dynamics from the those listed earlier in Eqns. 6-26. Instead, the direct collocation uses dynamics that pin the base to a ball joint at the global reference frame origin. This effectively eliminates the consideration of velocity terms for the torso. The equations which are modified from the simulation dynamics are shown below in Eqns. 36-43.

$$\mathbf{p}_t = L_{p2t}\mathbf{y}_0 \tag{36}$$

$$\mathbf{v}_t = \boldsymbol{\omega} \times \mathbf{p}_t \tag{37}$$

$$\dot{\mathbf{v}}_t = \tilde{\boldsymbol{\omega}}\, \mathbf{p}_t + \tilde{\boldsymbol{\omega}}^2 \mathbf{p}_t \tag{38}$$

$$\mathbf{J}_{b,\omega} = [\mathbf{I}_{3\times3} \quad \mathbf{0}_{3\times3}] \tag{39}$$

$$\mathbf{J}_{b,x} = \mathbf{0}_{3\times6} \tag{40}$$

$$\mathbf{J}_{i,\omega} = \begin{cases} [\mathbf{I}_{3\times3} \quad \mathbf{0}_{3\times3}] + \mathbf{y}_0 \mathbf{u}_{6,4}^T, & i = 0 \\ \mathbf{J}_{i-1,\omega} + \mathbf{x}_0 \mathbf{u}_{6,5}^T, & 1 \le i \le S_1 \end{cases} \tag{41}$$

$$\mathbf{J}_{i,com} = \mathbf{J}_{i,jnt} + \mathbf{J}_{i,j2c} \tag{42}$$

$$\mathbf{J}_{i,jnt} = \begin{cases} [-\tilde{\mathbf{p}}_t \quad \mathbf{0}_{3\times3}], & \mathbf{i = 1} \\ \mathbf{J}_{i-1} + \mathbf{J}_{i-1,j2j}, & \mathbf{i > 1} \end{cases}; \quad \begin{cases} \mathbf{J}_{i,j2c} = -\tilde{\mathbf{p}}_{j2c}\mathbf{J}_{i,\boldsymbol{\omega}} \\ \mathbf{J}_{i,j2j} = -\tilde{\mathbf{p}}_{j2j}\mathbf{J}_{i,\omega} \end{cases} \tag{43}$$

4.3 Single Shooting Method

Single shooting is another method of trajectory optimization which relies on simulation of the system. In this thesis the single shooting method used the simulation discussed in section 3.3.2 with the modification that the program now takes the parameters of link length and link mass as inputs. The same objective functions as shown in Eqs. 44-46 were used. As was done with the direct collocation method the *fmincon* in MATLAB was used to solve the optimization.

4.4 Optimization Results

The results reviewed here will be from the direct collocation method optimizing for an objective function that wishes to minimizing either control effort squared, or power squared throughout a maneuver and maximize the change in yaw achieved at the end of the maneuver. The cost function associated with control effort squared is shown in Eqn. 44, power squared is shown in Eqn. 45, and the common goal of maximizing yaw in Eqn. 46. These results will then be compared against results from the single shooting method given the same objective function. The single shooting results will be obtained by running single shooting with a cubic trajectory used in previous heuristic methods as well the optimal trajectory generated by the direct collocation method. All results will be validated in simulation to show differences in performance of the methods.

$$\min_{u_k} \sum_{k=0}^{N-1} \frac{1}{2}(h_k)(\mathbf{u}_k{}^2 + \mathbf{u}_{k+1}{}^2) \tag{44}$$

$$\min_{u_k} \sum_{k=0}^{N-1} \frac{1}{2}(h_k)((\mathbf{u}_k \cdot [\dot{\alpha} \quad \dot{\beta}]_k)^2 + (\mathbf{u}_{k+1} \cdot [\dot{\alpha} \quad \dot{\beta}]_{k+1})^2) \tag{45}$$

$$\min_{x_N} 1000\left(\frac{1}{\Phi_Z}\right)^2 \tag{46}$$

To begin with the direct collocation and single shooting methods were given the same cost function (Eqs. 44/45 and 46). The direct collocation had constraints implemented to restrict the final pitch and roll to be no greater than 5 degrees and $\dot{q}_N = 0$. This was done to help match the results of the cubic tail trajectory which the single shooting method first used. The direct collocation was set to have N=40. The optimization results are summarized in Table 4. Both optimizations used the same parameters for the body and had single segment tails with 18links. As can be seen from Table 4 and Figure 14 the single shooting method was able to achieve a much greater yaw but is overall a significantly less optimal design.

To help level the playing field between the single shooting and direct collocation method a second run of the single shooting method was done. This time the single shooting was given the optimal trajectory generated previously by the direct collocation in place of the original baseline cubic trajectory. The outputs from this can also be seen in Table 4. Again, the single shooting method picked a design which achieved greater yaw, but at the expense of significantly lower optimality owing to higher actuation efforts. Figure 15 shows that even with the closely matching tail bending motion the single shooting method still selects tail parameters that require significantly higher actuation effort.

Repeating these steps with the power squared cost function yields slightly different results. Due to either model inaccuracies or possibly errors caused by the fixed step trapezoidal integration, the direct collocation method comes up with a less optimal solution. The calculated costs are very similar between the single shooting cubic, single shooting with the direct collocation trajectory, and the direct collocation method, however. This is shown in Table 5. Figure 15 shows the difference in calculated roll torque from single shooting and direct collocation when following the same trajectory which likely causes the single shooting to show as performing better.

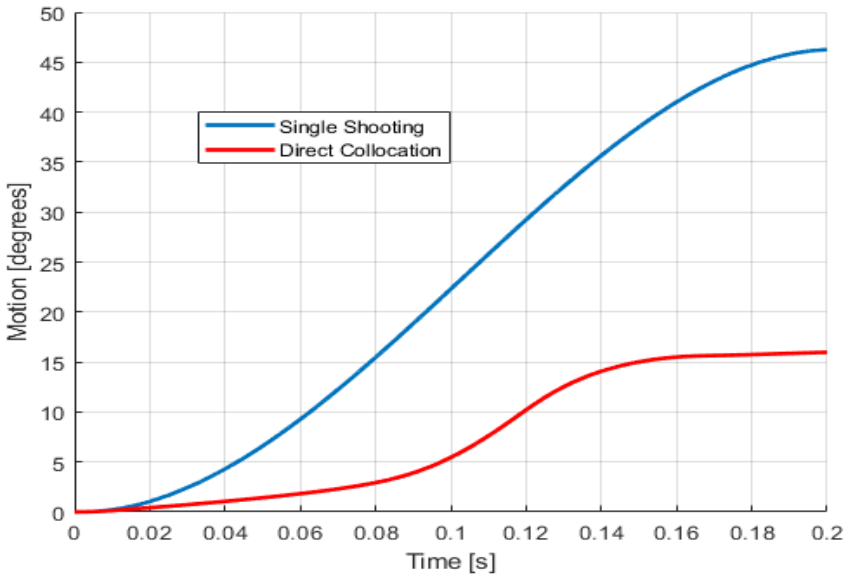

Figure 14 : Single Shooting vs. Direct Collocation

Table 4 : Optimization Results for Control Effort Squared

Output	Single Shooting	Direct Collocation	SS with DC Trajectory
Link Length [m]	.0640	.0265	.0528
Link Mass [kg]	.0867	.0046	.0100
Change in Yaw [Deg]	46.248	15.973	52.810
Peak Roll Torque [Nm]	.0007	.2726	.0027
Peak Cable Tension [N]	450.184	100.031	487.331
Cost Function Value [n/a]	936.513	53.718	1159.041

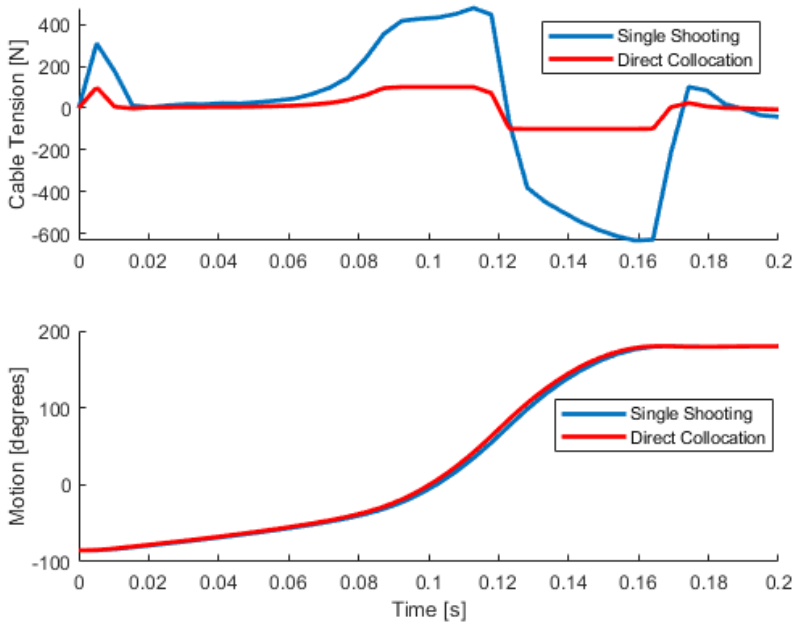

Figure 15 : Tail Bending Actuation Effort and Motion with Matched Control Effort Squared Trajectories

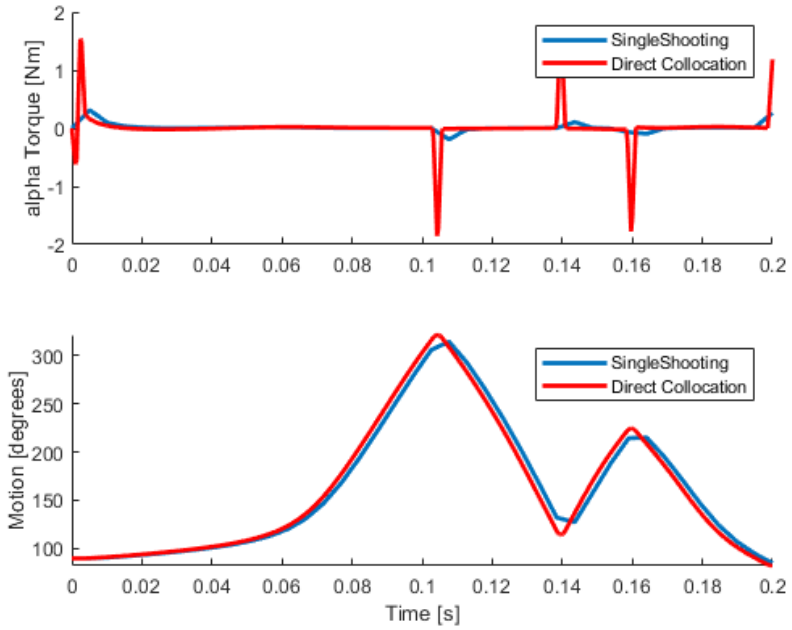

Figure 16 : Tail Roll Actuation Effort and Motion with Matched Power Squared Trajectories

Table 5 : Optimization Results for Power Squared

Output	Single Shooting	Direct Collocation	SS with DC Trajectory
Link Length [m]	.0576	.0389	.0376
Link Mass [kg]	.0100	.0143	.0100
Change in Yaw [Deg]	19.733	19.849	16.757
Peak Roll Torque [Nm]	0.000	1.8693	.0027
Peak Cable Tension [N]	59.451	171.41	130.29
Cost Function Value [n/a]	4.214	6.548	5.6223

The modified direct collocation method discussed is able to neatly meet the needs set out in the problem definition. The framework allows for optimization around a diverse set of scenarios due to its ability to implement boundary and path constraints. This does away with one of the most significant drawbacks of previous heuristic approaches which require reworking the entire setup to optimize for a new scenario. As is shown with the comparison to the single shooting method also helps to ensure that the tail design generated by the optimization will be compatible with trajectory optimizations which would traditionally be conducted after the design phase. It may appear as though the single shooting method provides better performance when only looking at the yaw motion output, but the direct collocation can be made to favor greater change in yaw over reduced actuation effort by changing the weights used in the cost functions.

5. CONCLUSION & FUTURE WORK

5.1 Summary

In this thesis a novel layout for a tail actuation unit which improves upon the existing R3RT architecture was presented. As well a new implementation of the direct collocation technique was proposed which allows for the addition of time invariant design parameters to be optimized alongside a trajectory.

The thesis began with a comprehensive literature review of existing tail designs and the design methodologies implemented to aid in their creation. The review highlighted the uses of tails and the advancements made in their structure and design. This motivates the need for an actuation unit which will allow for the continued testing and exploration of the abilities of serpentine tails when mounted to a mobile base. The review also served to show need for a more comprehensive and robust optimization methodology for serpentine tails.

Following the literature review an in-depth analysis of the proposed improved actuation unit was provided. This analysis started by presenting design targets generated based on simulation. Then, walked through the design of the compact and power dense actuators and tensioning mechanism which enable the novel spinal-esque layout. Finishing up Chapter 3, test results for both the standalone actuators as well as full tail system were presented to validate both the design and simulation used to generate the targets.

Following the actuation unit design, a discussion on the development of the new optimization method is given. The proposed method, which uses a modified direct collocation technique, along with a more traditional single shooting formulation were

presented. The results from these two techniques were then compared against each other and validated in simulation.

5.2 Future Work

Future work based on the findings of this thesis revolve primarily around continued prototype development and testing as well as expanding the optimization method to include a greater number of design parameters for the tail.

Testing of the actuation unit prototype has shown that the actuators have more than enough power to achieve highly dynamic movements. However, it has been discovered that the cable being used to actuate the tail is subject to stretch and that the tensioning system is not capable of accounting for this. Future work for the actuation unit should include the development of a more robust actuation unit and the identification of a better material for the tail actuation cable. Additionally, there is room to continue to reduce the size and weight of the actuators which would only serve to improve the overall performance of the system.

Results of the optimization method should be translated into prototype link designs so that further validation of the results can be conducted. As well the switch from *fmincon* to a different solver which can handle discrete integer variables would allow for the optimization to vary the number of links and segments in a tail. This could give even greater insight into designing optimal tails.

REFERENCES

[1] G. C. HICKMAN, "The mammalian tail: a review of functions," *Mammal review*, vol. 9, no. 4, pp. 143-157, 1979.

[2] J. W. Young, G. A. Russo, C. D. Fellmann, M. A. Thatikunta, and B. A. Chadwell, "Tail function during arboreal quadrupedalism in squirrel monkeys (Saimiri boliviensis) and tamarins (Saguinus oedipus)," *Journal of Experimental Zoology Part A: Ecological Genetics and Physiology*, vol. 323, no. 8, pp. 556-566, 2015.

[3] M. Bezanson, "The ontogeny of prehensile-tail use in Cebus capucinus and Alouatta palliata," *Am J Primatol*, vol. 74, no. 8, pp. 770-82, Aug 2012, doi: 10.1002/ajp.22028.

[4] S. M. O'Connor, T. J. Dawson, R. Kram, and J. M. Donelan, "The kangaroo's tail propels and powers pentapedal locomotion," *Biology letters*, vol. 10, no. 7, p. 20140381, 2014.

[5] C. Walker, C. J. Vierck Jr, and L. A. Ritz, "Balance in the cat: role of the tail and effects of sacrocaudal transection," *Behavioural brain research*, vol. 91, no. 1-2, pp. 41-47, 1998.

[6] A. M. Wilson, J. Lowe, K. Roskilly, P. E. Hudson, K. Golabek, and J. McNutt, "Locomotion dynamics of hunting in wild cheetahs," *Nature*, vol. 498, no. 7453, pp. 185-189, 2013.

[7] Y. Liu and P. Ben-Tzvi, "Dynamic modeling, analysis, and design synthesis of a reduced complexity quadruped with a serpentine robotic tail," *Integrative and Comparative Biology*, vol. 61, no. 2, pp. 464-477, 2021.

[8] W. Saab, W. S. Rone, and P. Ben-Tzvi, "Robotic tails: a state-of-the-art review," (in English), *Robotica*, Review vol. 36, no. 9, pp. 1263-1277, Sep 2018, doi: 10.1017/s0263574718000425.

[9] G. J. Zeglin, "Uniroo--a one legged dynamic hopping robot," Massachusetts Institute of Technology, 1991.

[10] F. J. Berenguer and F. M. Monasterio-Huelin, "Zappa, a quasi-passive biped walking robot with a tail: Modeling, behavior, and kinematic estimation using accelerometers," *IEEE Transactions on Industrial Electronics*, vol. 55, no. 9, pp. 3281-3289, 2008.

[11] A. Jusufi, D. T. Kawano, T. Libby, and R. J. Full, "Righting and turning in mid-air using appendage inertia: reptile tails, analytical models and bio-inspired robots," *Bioinspir. Biomim.*, vol. 5, no. 4, p. 045001, 2010.

[12] E. Chang-Siu, T. Libby, M. Tomizuka, and R. J. Full, "A lizard-inspired active tail enables rapid maneuvers and dynamic stabilization in a terrestrial robot," in *2011 IEEE/RSJ International Conference on Intelligent Robots and Systems*, 2011: IEEE, pp. 1887-1894.

[13] A. M. Johnson, T. Libby, E. Chang-Siu, M. Tomizuka, R. J. Full, and D. E. Koditschek, "Tail assisted dynamic self righting," in *Adaptive Mobile Robotics*: World Scientific, 2012, pp. 611-620.

[14] J. Zhao, T. Zhao, N. Xi, F. J. Cintrón, M. W. Mutka, and L. Xiao, "Controlling aerial maneuvering of a miniature jumping robot using its tail," in *2013 IEEE/RSJ International Conference on Intelligent Robots and Systems*, 2013: IEEE, pp. 3802-3807.

[15] G.-H. Liu, H.-Y. Lin, H.-Y. Lin, S.-T. Chen, and P.-C. Lin, "Design of a kangaroo robot with dynamic jogging locomotion," in *Proceedings of the 2013 IEEE/SICE International Symposium on System Integration*, 2013: IEEE, pp. 306-311.

[16] G.-H. Liu, H.-Y. Lin, H.-Y. Lin, S.-T. Chen, and P.-C. Lin, "A bio-inspired hopping kangaroo robot with an active tail," *Journal of Bionic Engineering,* vol. 11, no. 4, pp. 541-555, 2014.

[17] N. J. Kohut, A. O. Pullin, D. W. Haldane, D. Zarrouk, and R. S. Fearing, "Precise dynamic turning of a 10 cm legged robot on a low friction surface using a tail," in *2013 IEEE International Conference on Robotics and Automation*, 2013: IEEE, pp. 3299-3306.

[18] A. Patel and M. Braae, "Rapid turning at high-speed: Inspirations from the cheetah's tail," in *2013 IEEE/RSJ International Conference on Intelligent Robots and Systems*, 2013: IEEE, pp. 5506-5511.

[19] A. Patel and M. Braae, "Rapid acceleration and braking: Inspirations from the cheetah's tail," in *2014 IEEE International Conference on Robotics and Automation (ICRA)*, 2014: IEEE, pp. 793-799.

[20] W. R. Provancher, S. I. Jensen-Segal, and M. A. Fehlberg, "ROCR: An Energy-Efficient Dynamic Wall-Climbing Robot," *IEEE/ASME Transactions on Mechatronics*, vol. 16, no. 5, pp. 897-906, 2011, doi: 10.1109/tmech.2010.2053379.

[21] R. Briggs, J. Lee, M. Haberland, and S. Kim, "Tails in biomimetic design: Analysis, simulation, and experiment," in *2012 IEEE/RSJ International Conference on Intelligent Robots and Systems*, 2012: IEEE, pp. 1473-1480.

[22] E. Chang-Siu, T. Libby, M. Brown, R. J. Full, and M. Tomizuka, "A nonlinear feedback controller for aerial self-righting by a tailed robot," in *2013 IEEE International Conference on Robotics and Automation*, 2013: IEEE, pp. 32-39.

[23] A. De and D. E. Koditschek, "The Penn Jerboa: A platform for exploring parallel composition of templates," *arXiv preprint arXiv:1502.05347,* 2015.

[24] G. Wenger, A. De, and D. E. Koditschek, "Frontal plane stabilization and hopping with a 2DOF tail," in *2016 IEEE/RSJ International Conference on Intelligent Robots and Systems (IROS)*, 2016: IEEE, pp. 567-573.

[25] A. Shamsah, A. De, and D. E. Koditschek, "Analytically-Guided design of a tailed bipedal hopping robot," in *2018 IEEE/RSJ International Conference on Intelligent Robots and Systems (IROS)*, 2018: IEEE, pp. 2237-2244.

[26] A. Patel and E. Boje, "On the conical motion of a two-degree-of-freedom tail inspired by the cheetah," *IEEE Transactions on Robotics,* vol. 31, no. 6, pp. 1555-1560, 2015.

[27] W. Saab, P. Ben-Tzvi, and Asme, "DESIGN AND ANALYSIS OF A DISCRETE MODULAR SERPENTINE ROBOTIC TAIL FOR IMPROVED PERFORMANCE OF MOBILE ROBOTS," in *ASME International Design Engineering Technical Conference / Computer and Information in Engineering Conference (IDETC/CIE)*, Charlotte, NC, Aug 21-24 2016, NEW YORK: Amer Soc Mechanical Engineers, 2016.

[28] W. Saab, W. S. Rone, and P. Ben-Tzvi, "Discrete modular serpentine robotic tail: design, analysis and experimentation," (in English), *Robotica,* Article vol. 36, no. 7, pp. 994-1018, Jul 2018, doi: 10.1017/s0263574718000176.

[29] W. S. Rone, W. Saab, A. Kumar, and P. Ben-Tzvi, "Controller Design, Analysis, and Experimental Validation of a Robotic Serpentine Tail to Maneuver and *ASME,* Article vol. 141, no. 8, p. 9, Aug 2019, Art no. 081002, doi: 10.1115/1.4042948.

[30] W. Saab, S. Rone, A. Kumar, and P. Ben-Tzvi, "Design and Integration of a Novel Spatial Articulated Robotic Tail," (in English), *IEEE-ASME Trans. Mechatron.,* Article vol. 24, no. 2, pp. 434-446, Apr 2019, doi: 10.1109/tmech.2019.2897885.

[31] W. Rone, W. Saab, P. Ben-Tzvi, and Asme, "DESIGN, MODELING AND OPTIMIZATION OF THE UNIVERSAL-SPATIAL ROBOTIC TAIL," in *ASME International Mechanical Engineering Congress and Exposition*, Tampa, FL, Nov 03-09 2017, NEW YORK: Amer Soc Mechanical Engineers, 2018.

[32] W. S. Rone, W. Saab, and P. Ben-Tzvi, "Design, Modeling, and Integration of a Flexible Universal Spatial Robotic Tail," (in English), *J. Mech. Robot.,* Article vol. 10, no. 4, p. 14, Aug 2018, Art no. 041001, doi: 10.1115/1.4039500.

[33] Y. J. Liu, J. M. Wang, and P. Ben-Tzvi, "A Cable Length Invariant Robotic Tail Using a Circular Shape Universal Joint Mechanism," (in English), *J. Mech. Robot.,* Article vol. 11, no. 5, p. 14, Oct 2019, Art no. 051005, doi: 10.1115/1.4044067.

[34] Y. J. Liu and P. Ben-Tzvi, "Design, Analysis, and Integration of a New Two-Degree-of-Freedom Articulated Multi-Link Robotic Tail Mechanism," (in English), *J. Mech. Robot.,* Article vol. 12, no. 2, p. 9, Apr 2020, Art no. 021101, doi: 10.1115/1.4045842.

[35] Y. Liu and P. Ben-Tzvi, "Dynamic Modeling, Analysis, and Design Synthesis of a Reduced Complexity Quadruped with a Serpentine Robotic Tail," *Integrative and Comparative Biology,* 2021.

[36] Y. J. Liu and P. Ben-Tzvi, "Dynamic modeling, analysis, and comparative study of a quadruped with bio-inspired robotic tails," (in English), *Multibody Syst. Dyn.,* Article vol. 51, no. 2, pp. 195-219, Feb 2021, doi: 10.1007/s11044-020-09764-8.

[37] B. G. Katz, "A low cost modular actuator for dynamic robots," Massachusetts Institute of Technology, 2018.

[38] M. Kelly, "An introduction to trajectory optimization: How to do your own direct collocation," *SIAM Review,* vol. 59, no. 4, pp. 849-904, 2017.